

A theory of superconductivity in multi-walled carbon nanotubes

J. González¹ and E. Perfetto^{1,2}

¹*Instituto de Estructura de la Materia. Consejo Superior de Investigaciones Científicas. Serrano 123, 28006 Madrid. Spain.*

²*Istituto Nazionale di Fisica Nucleare - Laboratori Nazionali di Frascati, Via E. Fermi 40, 00044 Frascati, Italy.*

(Dated: February 8, 2020)

We devise an approach to describe the electronic instabilities of doped multi-walled nanotubes, where each shell has in general a manifold of Fermi points. Our analysis relies on the scale dependence of the different scattering processes, showing that a pairing instability arises for a large enough number of Fermi points as a consequence of their particular geometric arrangement. The instability is enhanced by the tunneling of Cooper pairs between nearest shells, giving rise to a transition from the Luttinger liquid to a superconducting state in a wide region of the phase diagram.

PACS numbers: 71.10.Pm, 74.50.+r, 71.20.Tx

Carbon nanotubes offer nowadays a great potential for the investigation of mesoscopic physics. It has been shown that they can have metallic or semiconducting properties, depending on the helicity of the carbon rings around the tubule¹. The electron correlations are moreover very strong in the carbon nanotubes, leading to the breakdown of the conventional Fermi liquid picture^{2,3,4,5}. This has become manifest, for instance, in the experimental observation of a power-law suppression of the conductance over a wide range of temperatures^{6,7}.

There have been also experiments showing the existence of superconducting (SC) correlations in the nanotubes at low temperatures. Supercurrents have been measured in nanotube ropes suspended between superconducting contacts⁸, showing genuine features of the transport of Cooper pairs in a 1D system⁹. Nanotube ropes have also displayed a sharp decrease in the resistance when suspended between nonsuperconducting electrodes¹⁰. Such transitions have been reported for samples with a large number (~ 300) of nanotubes, with critical temperatures below 1 K. More recently, quite abrupt drops in the resistance have been measured in large arrays of multi-walled nanotubes (MWNTs) grown in the pores of an alumina template¹¹. The ability to contact the top end of most part of the shells in the MWNTs seems to be crucial in this case, leading to transition temperatures of the order of ~ 10 K.

It arises the question of whether the SC transitions in the MWNTs can be understood on the same grounds as the superconductivity of the nanotube ropes¹². In the latter, the growth of the SC correlations takes place when the screened Coulomb interaction is overcome by the effective interaction mediated by phonons. For this to happen, a certain content of metallic nanotubes in a rope is required, as the Coulomb repulsion is more suppressed for larger number of conducting channels¹². In the MWNTs, the different shells may contribute to an efficient screening of the Coulomb interaction¹³, but an important drawback comes from the fact that the strength of the phonon-exchange interaction scales like the inverse of the nanotube radius¹⁴. On the other hand, the effect of doping must play an important role in the MWNTs, since it may ensure the metallic character of all the shells and

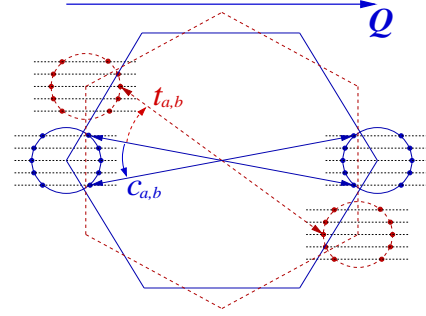


FIG. 1: Schematic representation of the location of the Fermi points for the shells of a doped MWNT, referred to the hexagonal Brillouin zone of graphene. The horizontal lines correspond to different low-energy subbands, arising from the conical dispersion around the vertices. The full (dashed) hexagon stands for the case of an armchair (zig-zag) geometry. The $c_{a,b}$ ($t_{a,b}$) couplings label the intratube (intertube) scattering of Cooper pairs at zero total momentum.

the possibility of Cooper-pair tunneling between them. In this perspective, the superconductivity of the MWNTs may be more related to that of the doped compounds of graphite, which have in some cases critical temperatures of the order of ~ 10 K¹⁵.

The aim of this paper is to study the low-energy instabilities of doped MWNTs, taking into account the different subbands crossing the Fermi level in each shell. These give rise to a manifold of Fermi points located in two disconnected patches in the reciprocal lattice, with an approximate circular shape as represented in Fig. 1. We will assume that the MWNTs are made of shells with a random mixture of helicities. In this model, single-electron tunneling between nearest shells must be largely suppressed since, in general, the misalignment of the respective carbon lattices leads to a relative rotation and to the mismatch of the Fermi points¹⁶, as shown in Fig. 1.

For typical shells with radius $R \sim 10$ nm, the energy spacing between the subbands is $\Delta E \sim 0.1$ eV. Below this energy, the different excitations are given by approximate linear branches around each Fermi point, corresponding to the dispersion in the longitudinal dimension.

In this regime the MWNTs behave as 1D conductors, and the electronic properties are dictated by the interaction among a collection of 1D electron liquids. This is consistent with the observation of Luttinger liquid behavior and the relative reduction of the exponent for the power-law dependence of the conductance in MWNTs¹⁷.

At energies much lower than ΔE , however, some of the interactions between the linear branches may grow large, pointing at the onset of an electronic instability in the system. This arises as a consequence of the particular arrangement of the manifold of Fermi points in each shell. We observe for instance that one patch is mapped into the other by a constant vector \mathbf{Q} , leading to an enhanced scattering with that momentum-transfer. In general, we will see that the anisotropy of the interactions bears a direct relation to the geometry of the disconnected patches, giving rise to a source of potential SC instability.

It is important then to analyze the scaling of the interactions at low energies, as usually done in 1D electron systems¹⁸. We classify first the interaction processes between electrons near respective Fermi points a and b with different left- and right-moving character (chirality) into (i) forward-scattering (with coupling $f_{a,b}^{(+)}$), when the particles remain around their respective Fermi points, and (ii) exchange (with coupling $f_{a,b}^{(-)}$), when the scattered particles exchange their positions around the Fermi points. Yet there is another type of interaction channel consistent with momentum conservation (Cooper-pair channel) in which two particles at opposite Fermi points a and $-a$ are scattered into another pair sitting at Fermi points b and $-b$. We will label the coupling for that process by $c_{a,b}^{(+)}$ ($c_{a,b}^{(-)}$) when the interacting particles keep (exchange) their chirality¹⁹.

The interaction vertices for the above channels are corrected by diagrams that depend logarithmically on the energy scale Λ , measured with respect to the Fermi level and running below the upper cutoff ΔE . This kind of divergence can be encoded into the scaling equations

$$\frac{\partial f_{a,b}^{(+)}}{\partial l} = -\frac{1}{2\pi v_{ab}}((f_{a,b}^{(-)})^2 - (c_{a,-b}^{(+)})^2) \quad (1)$$

$$\frac{\partial f_{a,b}^{(-)}}{\partial l} = -\frac{1}{\pi v_{ab}}((f_{a,b}^{(-)})^2 + (c_{a,-b}^{(-)})^2 - c_{a,-b}^{(-)}c_{a,-b}^{(+)}) \quad (2)$$

where $l = -\log(\Lambda)$ and the v_{ab} are defined in terms of the string of Fermi velocities v_a as $v_{ab} = (v_a + v_b)/2$. Regarding the couplings $c_{a,b}^{(\pm)}$, the scattering of the Cooper pairs is also enhanced by the fact that a pair with zero total momentum can be scattered within the same shell, or tunnel to a nearest shell and then back to the original nanotube. To describe these processes, new intertube tunneling couplings $t_{a,b}^{(\pm)}$ are required, standing for the amplitude of a pair (with momenta a and $-a$) to tunnel into another pair (with momenta b and $-b$) in the neighbor shell. To discern between the possible tunneling of singlet or triplet pairs, we assign an amplitude $t_{a,b}^{(-)}$ to the

process where the chiralities of the particles in the pair are exchanged, different to that for the direct process $t_{a,b}^{(+)}$. We have then the scaling equations

$$\frac{\partial c_{a,b}^{(+)}}{\partial l} = -\sum_{c,s} \frac{1}{2\pi v_c} (c_{a,c}^{(s)}c_{c,b}^{(s)} + t_{a,c}^{(s)}t_{c,b}^{(s)}) + \frac{1}{2\pi v_{ab}} c_{a,b}^{(+)} h_{a,b}^{(+)} \quad (3)$$

$$\begin{aligned} \frac{\partial c_{a,b}^{(-)}}{\partial l} = & -\sum_{c,s} \frac{1}{2\pi v_c} (c_{a,c}^{(s)}c_{c,b}^{(-s)} + t_{a,c}^{(s)}t_{c,b}^{(-s)}) \\ & -\frac{1}{\pi v_{ab}} c_{a,b}^{(-)} h_{a,-b}^{(-)} - \frac{1}{2\pi v_{ab}} \sum_s c_{a,b}^{(s)} h_{a,-b}^{(-s)} \end{aligned} \quad (4)$$

$$\frac{\partial t_{a,b}^{(\pm)}}{\partial l} = -\sum_{c,s} \frac{1}{2\pi v_c} (c_{a,c}^{(s)}t_{c,b}^{(\pm s)} + t_{a,c}^{(s)}c_{c,b}^{(\pm s)}) \quad (5)$$

with $h_{a,-b}^{(s)} \equiv 2f_{a,-b}^{(s)} - \delta_{ab}c_{a,a}^{(s)}$.

This model can be readily extended to include the tunneling beyond nearest-neighbor shells, but the main physical features are already described considering just the couplings $t_{a,b}^{(\pm)}$. These have nominally small values, fixed by the intertube distance, and their relative strength can be estimated by taking the square of the interlayer single-electron hopping in graphite, in units of the hopping rate in the graphene lattice. We obtain that the nominal relative amplitudes for tunneling are of the order of ~ 0.002 .

We remark that the model governed by the above equations has a sensible limit when the number N of coupled subbands becomes large, as a consequence of large nanotube radius (for the doped system). For different reasons, all the initial values of the couplings at the upper scale ΔE vanish at least as $1/N$ in the limit of large N . The bare Coulomb potential in each shell is given by³

$$V_C(\mathbf{r} - \mathbf{r}') = \frac{e^2/\kappa}{\sqrt{(x-x')^2 + 4R^2 \sin^2[(y-y')^2/2R^2] + a_z^2}} \quad (6)$$

with $a_z \simeq 1.6 \text{ \AA}$ and $\kappa \approx 2.4$. At small momentum-transfer, for instance, the screening by particle-hole excitations about all the Fermi points already produces a $1/N$ suppression of the dressed potential. Moreover, in the channels corresponding to $f_{a,b}^{(-)}$, the different symmetry of the Bloch wave functions for left- and right-moving electrons leads to an effective average of the interaction over the circumference of the tube, and to a $1/R$ reduction of its strength^{2,3,4}. The Coulomb potential for momentum-transfer about \mathbf{Q} suffers also a $1/R$ reduction, inherent to the behavior of the potential at large momentum. On the other hand, we recall that the 1D electron-phonon couplings are inversely proportional to the square root of the linear mass density²⁰, so that the effective potential due to phonon-exchange is overall reduced by a $1/R$ factor.

We observe therefore that the present approach to the electronic instabilities also makes sense in the case of thick MWNTs. In these conditions, all the couplings are in the weak-coupling regime, and the model is still able

to describe interesting physical effects as the number of contributions to the right-hand-side of Eqs. (3)-(5) grows with N , compensating the smallness of the couplings.

We have solved the scaling equations in a wide range of physical conditions, corresponding to different values of (i) the average radius of different shells in the MWNT, and (ii) the doping level, represented by the shift $\Delta\varepsilon_F$ in the Fermi energy. In this task, we have first computed the Coulomb contribution to the initial value of each coupling, dressing the potential (6) at small momentum-transfer by the RPA sum of particle-hole processes from different shells and subbands. Regarding the contribution of the phonon-mediated interaction, we have relied on the results obtained for nanotubes in a wide range of diameters^{21,22}, which coincide in the observation that the effective coupling λ for small momentum-transfer is about three times smaller (in absolute value) than that for momentum about \mathbf{Q} . This relation is also obeyed by the couplings in a graphite layer²³. We have thus taken a contribution to the initial couplings from phonon-exchange running between $\lambda = -0.1/R$ and $-0.03/R$ (with R expressed in \AA) for the channels with small momentum-transfer, and respective values equal to 3λ for the channels with momentum-transfer about \mathbf{Q} ^{21,22}.

In order to characterize low-energy instabilities, we have computed the different response functions for operators corresponding to order parameters for all types of symmetries (charge-density-wave (CDW), spin-density-wave, superconductivity with various wave symmetries). Each SC response function $R_g(\omega)$ for given g -wave symmetry, for instance, has a derivative with respect to the frequency $\bar{R}_g = \partial R_g / \partial \log \omega$, that satisfies an scaling equation¹⁸

$$\frac{\partial \bar{R}_g(\Lambda)}{\partial \log(\Lambda)} = \sum_{a,b,s} g_{a,b}^{(s)} c_{a,b}^{(s)}(\Lambda) \bar{R}_g(\Lambda) \quad (7)$$

where $g_{a,b}^{(s)}$ is the symmetry factor appropriate for each particular wave. We have observed that there is a region of the phase diagram, represented in Fig. 2, where the growth of the SC response functions is overshadowed by the divergence of any of the CDW response functions at low energies. Above the phase boundary shown in the figure, however, the CDW correlations are small and the instability is dictated by the large growth of the intertube couplings $t_{a,b}^{(s)}$. This is the signal that the Cooper pairs are able to propagate across the entire multi-walled structure. The 3D Cooper-pair propagator $P_g(\omega)$ can be obtained as a ladder sum of multiple intertube tunneling processes, $P_g(\omega) \approx R_g(\omega)/(1 - \sum g_{a,b}^{(s)} t_{a,b}^{(s)} R_g(\omega))$. The pole of $P_g(\omega)$ at some finite frequency ω_c marks the transition to a SC state, that we have always found in a channel of p -wave symmetry (together with subdominant d -wave pairing correlations).

There is a natural explanation for the appearance of SC correlations with p -wave symmetry, which relies on the peculiar arrangement of the Fermi points into two circular patches. These have a symmetry that corresponds to

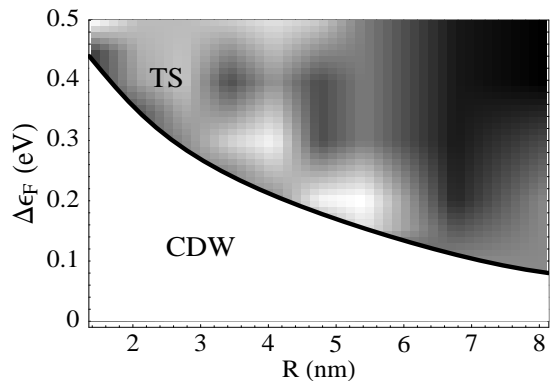


FIG. 2: Phase diagram of doped MWNTs in terms of the average radius R of the shells and the doping level, represented by the shift $\Delta\varepsilon_F$ in the Fermi energy. The upper region corresponds to a SC phase with p -wave symmetry. The density plot represents in grey scale the values of the logarithm of the transition scale ω_c (in units of ΔE), ranging from $-\log \omega_c \approx 4$ (black) to ≈ 6 (white).

the group C_{2v} . The Cooper-pair vertex, taken as a function of the angular variables θ and θ' of the pairs before and after the scattering, may be expanded in the form

$$V(\theta, \theta') = V_0 + V_1 \cos(\theta) \cos(\theta') + V_2 \sin(\theta) \sin(\theta') + V_3 \cos(2\theta) \cos(2\theta') + V_4 \sin(2\theta) \sin(2\theta') \quad (8)$$

A simple operation allows to estimate the different coefficients in the expansion. By placing one of the electrons in the incoming pair at the maximum angle θ_0 spanned by one circular patch, we may parametrize V_1, V_2, V_3 and V_4 in terms of the values of the vertex at zero momentum-transfer, $V(\theta_0, \theta_0) \equiv U_1$, at \mathbf{Q} momentum-transfer, $V(\theta_0, \pi - \theta_0) \equiv U_2$, with incoming and outgoing electrons at opposite angles, $V(\theta_0, -\theta_0) \equiv U_3$, and at antipodal points, $V(\theta_0, \pi + \theta_0) \equiv U_4$. We obtain

$$V_1 \cos^2(\theta) = (U_1 - U_2 + U_3 - U_4)/4 \quad (9)$$

$$V_2 \cos^2(\theta) = (U_1 + U_2 - U_3 - U_4)/4 \quad (10)$$

$$V_4 \cos^2(2\theta) = (U_1 - U_2 - U_3 + U_4)/4 \quad (11)$$

The key point is that, due to the large number of particle-hole excitations from the many Fermi points in a shell, the interactions with very small longitudinal momentum-transfer are more screened than those with some transverse (as opposed to longitudinal) momentum within the same circular patch. This means that $U_1 < U_3$, so that an attractive interaction may exist in the Cooper-pair channels with p -wave (V_2) and d -wave (V_4) symmetry. We recall that, as homologous Fermi points in the two circular patches can be connected by the fixed vector \mathbf{Q} , the screening is also enhanced for that particular momentum. This implies that $U_2 < U_4$, leading from Eq. (10) to $V_2 < 0$. This is the origin of the electronic instability, as an attractive interaction in one of the pairing channels is always driven to strong-coupling in the low-energy limit.

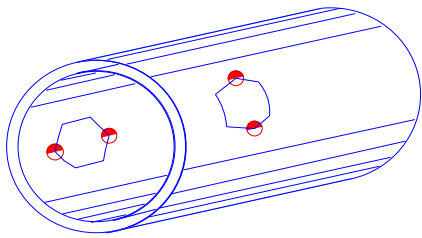


FIG. 3: Schematic representation of the orientation of the nodal line (dividing colored and white sectors of the circular patches of Fermi points around the corners of the Brillouin zone) for nearest shells with armchair and zig-zag geometry.

We have seen that the combination of signs of the couplings $t_{a,b}$ in the low-energy limit is such that it favours a p -wave symmetry of the pair wave function, with the nodal line being perpendicular to the line dividing left- and right-moving modes in the circular patches. We stress that such a symmetry arises from the larger repulsion felt when the momentum-transfer has some transverse component. Although the helicity of nearest shells may be different and the respective Brillouin zones may have a relative rotation, as shown in Fig. 1, the nodal line keeps always the same orientation from shell to shell, as it turns out to be anyhow parallel to the longitudinal dimension of the nanotube. This is illustrated in Fig. 3 for the particular case of armchair and zig-zag shells. The propagation of the Cooper pairs with the mentioned p -wave symmetry can be thus maintained consistently through the tunneling processes, in spite of the random mixture of helicities that may be present in a MWNT.

We have thus developed an approach that is suitable to describe the electronic instabilities of doped MWNTs, which may have many subbands at the Fermi level. This

analysis may be relevant to account for the signatures of SC transitions reported in Ref. 11. Our approach relies on the scale-dependence of different scattering processes at low energies, and it allows to describe the transition from the Luttinger liquid to a SC state as some of the Cooper-pair couplings start to grow large.

The scale of the transition, determined by the point ω_c at which the 3D Cooper-pair propagator $P_g(\omega)$ has a pole, ranges in the phase diagram of Fig. 2 between values corresponding to $-\log(\omega_c/\Delta E) \approx 4 - 6$. Recalling that $\Delta E \sim 0.1$ eV, we find that the critical temperature can be between a lower scale of ~ 1 K and a higher scale of ~ 10 K. This range of variation is maintained up to the largest radii for which we have solved the model (demanding up to ~ 50 Fermi points and $\sim 1,000$ independent couplings). This suggests that the superconductivity observed in the MWNTs may be related to that of doped graphite²⁴, where values of the critical temperature up to ≈ 11 K have been reported¹⁵.

We have shown that the mechanism of superconductivity in doped MWNTs is based on the particular geometry of the two patches of Fermi points. A reflection of this is the appearance of the SC instability in a channel of p -wave symmetry. It is tempting to relate this feature to the observation of the interplay between SC and magnetic order parameters in some samples of doped graphite²⁵. All these properties should deserve further investigation at the experimental level, for the sake of clarifying as well the relation between the superconductivity of different carbon compounds.

The financial support of the Ministerio de Educación y Ciencia (Spain) through grant FIS2005-05478-C02-02 is gratefully acknowledged. E. P. was also supported by INFN grant 10068.

-
- ¹ N. Hamada, S. Sawada and A. Oshiyama, Phys. Rev. Lett. **68**, 1579 (1992). R. Saito *et al.*, Appl. Phys. Lett. **60**, 2204 (1992).
- ² L. Balents and M. P. A. Fisher, Phys. Rev. B **55**, R11973 (1997).
- ³ R. Egger and A. O. Gogolin, Phys. Rev. Lett. **79**, 5082 (1997); Eur. Phys. J. B **3**, 281 (1998).
- ⁴ C. Kane, L. Balents and M. P. A. Fisher, Phys. Rev. Lett. **79**, 5086 (1997).
- ⁵ H. Yoshioka and A. A. Odintsov, Phys. Rev. Lett. **82**, 374 (1999); Phys. Rev. B **59**, R10457 (1999).
- ⁶ M. Bockrath *et al.*, Nature **397**, 598 (1999).
- ⁷ Z. Yao *et al.*, Nature **402**, 273 (1999).
- ⁸ A. Yu. Kasumov *et al.*, Science **284**, 1508 (1999).
- ⁹ J. González, Phys. Rev. Lett. **87**, 136401 (2001).
- ¹⁰ M. Kociak *et al.*, Phys. Rev. Lett. **86**, 2416 (2001).
- ¹¹ I. Takesue *et al.*, Phys. Rev. Lett. **96**, 057001 (2006).
- ¹² J. González, Phys. Rev. Lett. **88**, 076403 (2002).
- ¹³ R. Egger, Phys. Rev. Lett. **83**, 5547 (1999).
- ¹⁴ A. De Martino and R. Egger, Phys. Rev. B **67**, 235418 (2003).
- ¹⁵ N. Emery *et al.*, Phys. Rev. Lett. **95**, 087003 (2005).
- ¹⁶ A. A. Maarouf, C. L. Kane and E. J. Mele, Phys. Rev. B **61**, 11156 (2000).
- ¹⁷ A. Bachtold *et al.*, Phys. Rev. Lett. **87**, 166801 (2001).
- ¹⁸ J. Sólyom, Adv. Phys. **28**, 201 (1979).
- ¹⁹ A similar analysis has been applied to investigate the instabilities in a 2D square lattice by H.-H. Lin, L. Balents and M. P. A. Fisher, Phys. Rev. B **56**, 6569 (1997).
- ²⁰ D. Loss and T. Martin, Phys. Rev. B **50**, 12160 (1994).
- ²¹ A. Sédéki, L. G. Caron and C. Bourbonnais, Phys. Rev. B **65**, 140515 (2002).
- ²² D. Connétable *et al.*, Phys. Rev. Lett. **94**, 015503 (2005).
- ²³ S. Piscanec *et al.*, Phys. Rev. Lett. **93**, 185503 (2004).
- ²⁴ L. X. Benedict *et al.*, Phys. Rev. B **52**, 14935 (1995).
- ²⁵ S. Moehlecke, Y. Kopelevich and M. B. Maple, Phys. Rev. B **69**, 134519 (2004).